Nanoscale Advances

rsc.li/nanoscale-advances

ROYAL SOCIETY
OF CHEMISTRY

NCNST

COMMUNICATION
Shan Jiang *et al.*
Biobased superhydrophobic coating enabled by
nanoparticle assembly

COMMUNICATION

Check for updates

Biobased superhydrophobic coating enabled by nanoparticle assembly†

Emily Olson,[ab] Jonathan Blisko, [ID][c] Chuanshen Du,[a] Yi Liu,[d] Yifan Li,[a]
Henry Thurber,[ab] Greg Curtzwiler, [ID][be] Juan Ren,[d] Martin Thuo, [ID][a] Xin Yong [ID][c]
and Shan Jiang [ID] *[ab]

Understanding biobased nanocomposites is critical in fabricating high performing sustainable materials. In this study, fundamental nanoparticle assembly structures at the nanoscale are examined and correlated with the macroscale properties of coatings formulated with these structures. Nanoparticle assembly mechanisms within biobased polymer matrices were probed using *in situ* liquid-phase atomic force microscopy (AFM) and computational simulation. Furthermore, coatings formulated using these nanoparticle assemblies with biobased polymers were evaluated with regard to the hydrophobicity and adhesion after water immersion. Two biobased glycopolymers, hydroxyethyl cellulose (HEC) and hydroxyethyl starch (HES), were investigated. Their repeating units share the same chemical composition and only differ in monomer conformations (α- and β-anomeric glycosides). Unique fractal structures of silica nanoparticle assemblies were observed with HEC, while compact clusters were observed with HES. Simulation and AFM measurement suggest that strong attraction between silica surfaces in the HEC matrix induces diffusion-limited-aggregation, leading to large-scale, fractal assembly structures. By contrast, weak attraction in HES only produces reaction-limited-aggregation and small compact cluster structures. With high particle loading, the fractal structures in HEC formed a network, which enabled a waterborne formulation of superhydrophobic coating after silane treatment. The silica nanoparticle assembly in HEC was demonstrated to significantly improve adhesion, which showed minimum adhesion loss even after extended water immersion. The superior performance was only observed with HEC, not HES. The results bridge the assembly structures at the nanoscale, influenced by molecular conformation of biobased polymers, to the coating

performance at the macroscopic level. Through this study we unveil new opportunities in economical and sustainable development of high-performance biobased materials.

Introduction

Biobased materials aim to provide sustainable alternatives to traditionally petroleum derived materials, such as coatings, adhesives, and construction chemicals.[1–4] Beyond the raw material cost, limited performance inhibits the replacement of petroleum-based polymers by their biobased counterparts. Taking coating materials as an example, the properties of biobased coatings must be improved, particularly their mechanical strength and water resistance.[5–7] One approach to build new functionality and improve performance is to fabricate biobased nanocomposites.[8–11] Nanoparticles have already been widely used to enhance the performance of the polymer matrix. Extensive research has been reported with petroleum based polymer matrices, though far fewer studies have been carried out with biobased polymer matrices.[12,13] More importantly, the understanding of molecular structures and interactions within biobased polymers is very limited, as these polymers often possess complicated architectures and vary from different parent sources.[14–18] The fundamental study and systematic comparison of nanoparticle assembly structures within different biopolymers are needed to provide insight on the interactions and assembly mechanism.

Nanoparticles in polymer matrices can assemble into a number of structures ranging from clusters to networks and films.[19–23] Their assembly is dictated by intermolecular forces, such as hydrogen bonding, electrostatic and van der Waals forces.[24–26] The aforementioned forces vary in magnitude and depend on interparticle distance. In addition, polymer morphology and entropy (depletion force) may play important roles in modulating interparticle interactions.[27–32] To probe interparticle interactions and assembly mechanisms within

[a]Department of Materials Science and Engineering, Iowa State University, Ames, IA 50011, USA. E-mail: sjiang1@iastate.edu

[b]Polymer and Food Protection Consortium, Iowa State University, Ames, IA 50011, USA

[c]Department of Mechanical Engineering, Binghamton University, Binghamton, NY 13902, USA

[d]Department of Mechanical Engineering, Iowa State University, Ames, IA 50011, USA

[e]Department of Food Science and Human Nutrition, Iowa State University, Ames, IA 50011, USA

biobased polymers, we adopt integrated advanced tools, including liquid-phase atomic force microscopy (AFM) and computational simulation. In *in situ* AFM, a fluid environment can be used to replicate the wet condition, where adhesion is measured with a microscale colloidal probe mounted on the scanning tip.[33] With a substrate opposite the probe, we can directly measure the adhesion and deflection forces between the two surfaces in polymer solutions as the probe approaches and retreats from the substrate. To further verify that the observed nanoparticle assembly structures indeed originate from interparticle forces, computational simulation is utilized to corroborate the force measurement with the assembly structures. So far, force measurement, theory, and simulation models on biobased polymers and their nanocomposites are scarce.[34]

In this study, drastically different assembly structures of silica nanoparticles were observed in two biobased polymers, hydroxyethyl starch (HES) and cellulose (HEC). These polymers were correspondingly derived from starch and cellulose by randomly modifying the side hydroxy groups with hydroxyethyl groups. The minor modification (1.3–5 molar substitution) destroyed the crystallinity and renders these polymers completely water soluble.[35] HEC and HES share very similar monomer molecular structures that differ only in the orientation of glycosidic hydroxyethyl pendant groups. Intriguingly, the differences in chain conformation between HES and HEC mediate the formation of drastically different assembly structures of silica nanoparticles. In the coiled, *cis* conformation of HES matrix, silica nanoparticles formed close packed clusters. While in the extended, *trans* conformation of HEC, the same nanoparticles formed loose fractal structures. Liquid-phase AFM detected the obvious difference in interactions between silica surfaces within HEC and HES aqueous solutions. Based on the input from the force measurement, computational simulation successfully reproduced structures resembling the experimental observation.

Utilizing the knowledge obtained from fundamental studies of HEC and HES polymers, we further applied the resulting nanoparticle assembly structures to achieve a waterborne formulation and create superhydrophobic coatings. A major challenge in developing a biobased waterborne coating system is to improve the water repellency, especially with water dispersible polymers. Approaches have been developed to impart hydrophobicity to polymers *via* surface treatments and controlling surface roughness.[36] Surface treatments often refer to silane vapor deposition or liquid cast.[37–41] Surface roughness can be fabricated *via* colloidal lithography,[42] hot press,[43–45] mould,[46–48] and selective evaporation.[49] In addition, switchable hydrophilic and hydrophobic patterns have been designed for lotus-like self-cleaning capabilities.[50–53] However, most of these methods require complicated fabrication and surface treatment, which often involve chemical reactions in organic solvent.[54–59] It is much more challenging to create a durable hydrophobic surface using simple and straightforward waterborne coating formulations. Taking advantage of the unique nanoparticle assemblies discovered in this study, we have created a waterborne formulation that can provide both superhydrophobicity and strong adhesion even after water immersion. In doing so, we offer solutions to address ongoing challenges in biobased polymer applications, including water resistance and adhesion performance. The results will inspire new opportunities for applying biobased materials to many more areas of study, including inks, additive manufacturing, and biomedical devices.

Experimental

Chemicals

Tetraethyl orthosilicate (Sigma Aldrich, 99.999%), cyclohexane (Fischer Scientific, ≥99%), ammonia hydroxide (ACROS Organics, Extra Pure), ethanol (Fischer Scientific, 100%), hydroxyethyl cellulose (Sigma Aldrich, 90 000 g mol^{-1}), hydroxyethyl starch (Sigma Aldrich, 200 000 g mol^{-1}), (1*H*,1*H*,2*H*,2*H*-perfluorooctyl)silane (Sigma Aldrich, 97%), octyltrichlorosilane (Sigma Aldrich, 97%), rhodamine B iso-thiocyanate (Sigma Aldrich), ammonium persulfate (Sigma Aldrich, ≥98%), L-arginine (Sigma Aldrich, ≥98%), hydrochloric acid (Fischer Scientific, 36.5–38%).

Silica synthesis

Silica dioxide nanoparticles were synthesized according to a modified Stöber method. Briefly, 140 mL water and 146 mg L-arginine were added to a 500 mL Erlenmeyer flask. 30 mL of cyclohexane was added to serve as the organic layer. The solution was capped, then stirred slowly at 65 °C. Following, 11.2 mL of TEOS was added, and the mixture was allowed to react for 20 hours. To stop the reaction 0.1 mL of HCl was added. The silica nanoparticles were collected *via* washing and centrifugation. Particle size is recorded as 100 nm. To fluorescently label the particles, the previous method was modified to include a dye. The dye was synthesized by combining 5.44 mg rhodamine B isothiocyanate with 20 mL of ethanol and 8.99 mg of ammonium persulfate. The mixture was covered with foil and shaken for 8 hours. To make the labelled silica, the synthesis process was repeated as stated above, with the addition of 1 mL fluorescent dye prior to the 20 hour reaction time.

Coating formulation

In a glass vial, hydroxyethyl starch/cellulose (1.2 g) was diluted to 4 wt%. The polymer molecular weights were selected to match viscosity at similar polymer concentration. The mixture was stirred at 550 rpm, adjusted to pH 9 with ammonia hydroxide, and stirred once more. The solution was then heated under microwave irradiation to better dissolve the polymer. Following, a separate mixture of silica dioxide nanoparticles (0.16–3 wt%) and deionized water (0.95 mL) was stirred and sonicated. The solution was diluted with deionized water (3 mL), stirred, and then homogenized. The formulation was drawn down on corona-treated polyethylene plastic (or aluminum Q-panels) with a stainless steel drawdown bar of 75 μm wet thickness.

Silane treatment

Salinization of surfaces were conducted similar to previous described.[60] The sample was first secured in a clean, dry desiccator with 100 μL of alkylsilane in a 10 mL clean glass vial secured inside the desiccator. The desiccator was then sealed, evacuated, and transferred to a pre-heated oven (45 °C) for reaction for 3 hours. Octyltrichlorosilane or trichloro(1H,1H,2H,2H-perfluorooctyl)silane were used, while both of the 97% silanes were purchased from Sigma-Aldrich and used as received.

AFM

In-liquid force curve measurements were performed on a commercial AFM platform (BioResolve, Bruker Inc.). Sphere silica probes with nominal diameter of 5 μm were used. To avoid cross contamination, each probe was only used in one type of liquid. The spring constant of each AFM cantilever was calibrated using thermal tune approach before the force measurements.[33] All the force–distance curves were obtained at the ramp frequency of 1 Hz. The force vs. distance data were exported from the AFM software (Nanoscope, Bruker Inc.) and replotted in Matlab (Mathworks) for comparison.

Simulation

Computer simulations of nanoparticle assembly in the HEC and HES solutions were performed on the mesoscale using Langevin dynamics. Nanoparticles were modeled as coarse-grained Brownian particles with their individual dynamics resolved. The polymer solution was modeled implicitly as a continuum that influences interparticle interactions and exerts stochastic and frictional forces on particles. The effective interaction potentials of nanoparticles in the two polymer solutions were developed based on the corresponding AFM force measurement. A geometric scaling was conducted to obtain the pairwise forces between particles of size 100 nm from the AFM data measured with the microscale colloidal probe (Fig. S3†). The resulting interparticle potential energies for the HEC and HES systems were fitted to polynomials and subsequently employed in the Langevin dynamics simulation. The reversible assembly of nanoparticles was simulated through a two-step Metropolis Monte Carlo scheme coupled to the Langevin dynamics. The assembled clusters continue their movement as rigid bodies with translational and rotational diffusion. Both aggregation and separation events were incorporated for allowing the relaxation of assembly structures under the effect of thermal fluctuations. Additional details of force scaling and simulation methods are described in the ESI.†

Characterization

Scanning electron microscope micrographs were obtained via a field-emission scanning electron microscope (Nanonova 230, FEI, secondary electron). Wet tracking of fluorescent silica (excitation wavelength: 570 nm, emission wavelength: 575 nm) was assessed via the use of a digital microscope (Leica DVM6) with a glass bottom well plate. Water repellency was measured

with a goniometer (Ramé-Hart 200 (p/n 200-U1)) using 1 μL of deionized water. Contact angle images were collected with a high-resolution camera and analyzed with DROPimage software. Laser light diffraction was measured with a dynamic light scattering (Zetasizer NanoZS, Malvern). Adhesion measurements were conducted via ASTM 3359 with a crosshatch knife kit.

Results and discussion

In our nanoparticle assembly study, there are only two major components: the biobased polymer matrix and nanoparticles. This simple combination offers a model system in understanding how polymers drive the formation of complex assembly structures. For the matrix, hydroxyethyl modified cellulose (HEC) and starch (HES) polymers were used. To best capture the interactions in the silica nanoparticle suspension, in situ liquid phase AFM was performed. The colloidal probe was equipped with a glass bead, and the polymer solution (of HEC or HES) was added to a Petri dish with the glass bottom. With this setup, we can reproduce the silica–silica surface interactions in presence of polymer. The contrast in magnitude and range of forces between silica surfaces in HEC and HES is clearly demonstrated by the AFM measurement. The results of the experiment reveal a four-fold difference in attraction force between silica surfaces within HEC (1.0×10^{-10} N) and HES (2.5×10^{-11} N) polymer matrices (Fig. 1a). In addition, the distance range at which the attractive force persists is two times larger in HEC (~100 nm) than in HES (~50 nm). This means that there is a stronger force dictating silica interactions when HEC is used as the matrix. The discovery is intriguing as these polymers are almost identical in chemical composition but only differ in orientation of the anomeric bonds (Fig. 1a inset). Based on the force measurement, the potentials between two silica particles were derived (Fig. 1b).

The primary conformation of HEC and HES is likely consistent with their cellulose and starch parent structures. The hydroxyethyl pendant groups limit movement and determine the conformation of the primary chain. The cellulose derivative has trans linkages (α-anomer), which separate the bulky pendant groups and allow the polymer to take on an extended conformation. On the other hand, hydroxyethyl starch has cis linkages (β-anomer), which place the hydroxyethyl groups in adjacent units close to each other, pushing the polymer to a coil conformation (Fig. 1a inset). Therefore, the persistence lengths of starch and cellulose vary due to the orientation of the pendant alcohol groups. For starch, the persistence length is 6 nm due to the cis conformation.[61] By contrast, in cellulose structures, the trans conformation leads to an extended persistence length of 40 nm.[62] The extended conformation of HEC may help induce a stronger and longer attractive force between silica surfaces than HES, due to possible bridging and hydrogen bonding. Interestingly, the orientation of the pendant groups on the polymer backbone and chain conformation also have dramatic impacts on assembly structures of nanoparticles within the matrix.
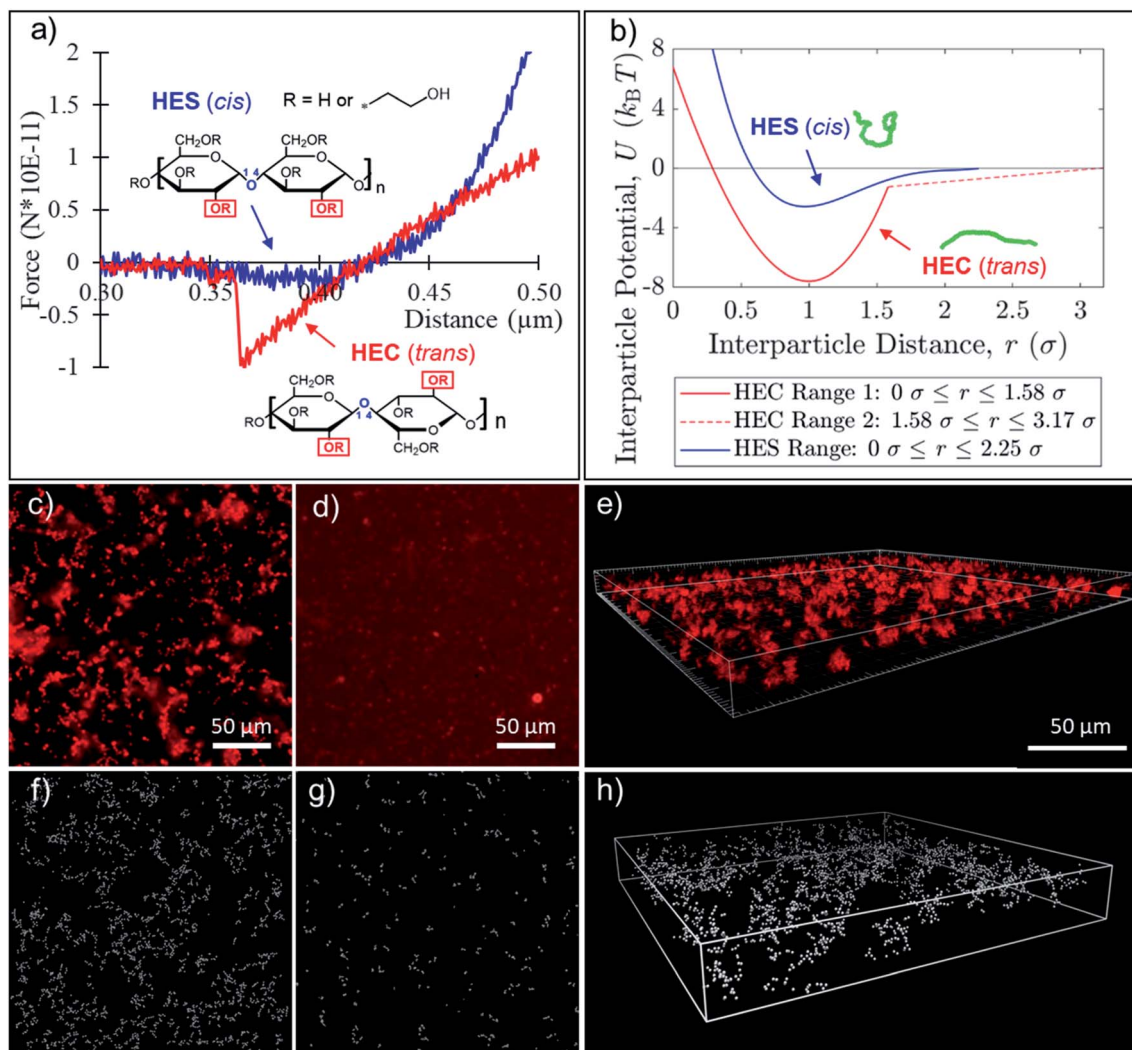
Fig. 1   (a) *In situ* AFM colloidal force measurement between silica surfaces in HEC and HES solution, inset shows the molecular structure of HEC and HES; (b) potential between silica nanoparticles in HEC and HES solution derived from AFM results, inset shows the difference in chain conformation between HEC and HES; (c) fluorescent microscopy of silica nanoparticles in HEC solution; (d) fluorescent microscopy of silica nanoparticles in HES solution; (e) confocal 3D image of silica nanoparticle assembly in HEC; (f) simulation result of nanoparticle assembly in HEC; (g) simulation result of nanoparticle assembly in HES; (h) image of 3D view nanoparticle assembly in HEC by simulation.

To track the assembly, the formulations were prepared in a closed system to mitigate any influence of evaporation. A dilute (0.16 wt%) suspension of fluorescently labelled silica nanoparticles (100 nm), initially dispersed, was allowed to self-assemble and observed *in situ* under a fluorescent microscope. The formation of a loose fractal structure was clearly observed in the HEC suspension within 12 hours (Fig. 1c). However, nanoparticles form small compact clusters in the HES suspension (Fig. 1d). Confocal laser scanning microscope further revealed the three-dimensional assembly structures (Fig. 1e). The comparison of nanoparticle assemblies at longer time point (24 hours) in Fig. S1† consistently demonstrates the same trend as observed in 12 hours. In the HEC suspension, nanoparticles form larger fractal network clusters. Alternatively, HES remains dispersed as compact clusters throughout the 24 hour time lapse, only slightly settling to the substrate as time progresses. The difference in nanoparticle assembly structures in the

aqueous suspension can also be viewed clearly even after solution is dried into a coating film. With dilute (0.16 wt%) concentrations of silica nanoparticles, we observe the formation of a fractal network structure in presence of HEC (4 wt%) in the dried film (Fig. S2†). By contrast, nanoparticles are dispersed as clusters in HES (4 wt%) matrices.

To further study how differences in polymer–particle interactions within HEC and HES suspension could translate into the difference in nanoparticle assembly structures, computational modeling and simulation were carried out. Simulation parameters were established based on the AFM force measurement (Fig. 1b and S3†). It is important to note that nanoparticles assemblies in HEC suspension sediment faster to the bottom of the container than individual nanoparticles due to differences in effective gravity. Through fluorescent intensity measurement, it is estimated that the concentration of nanoparticles in Fig. 1c is ~0.8%, while concentration of
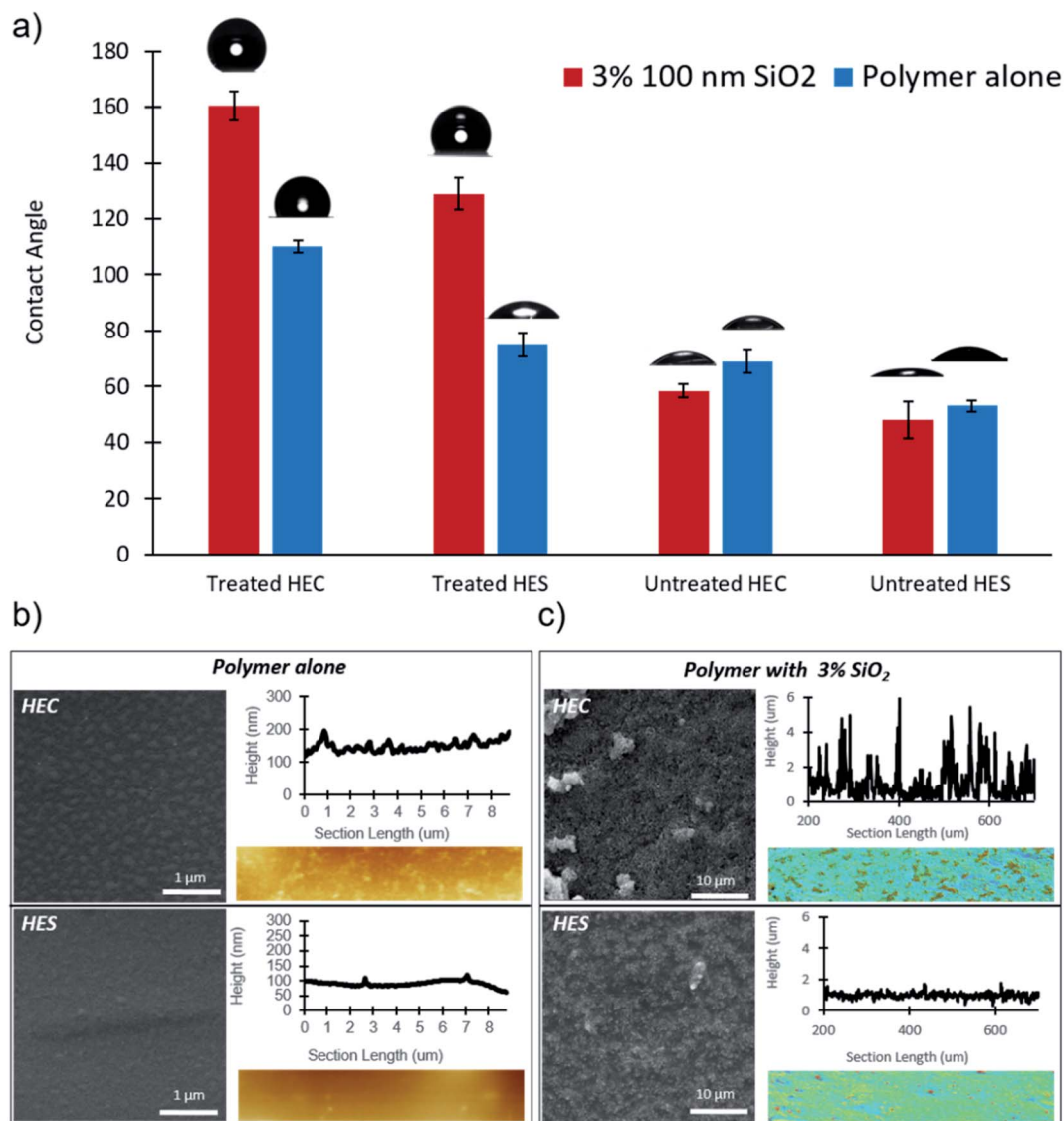
Fig. 2 (a) Contact angle measurement of nanocomposite coating films made from HEC and HES, both treated and untreated; (b) SEM micrographs and AFM topography profiles of polymer alone samples; (c) SEM micrographs and confocal profiles of nanocomposite samples.

nanoparticles in Fig. 1d is ~0.16%. Therefore, these different concentration values were used in simulation for HEC and HES, correspondingly, to capture the experimental conditions more accurately. The simulation successfully replicated the experimentally observed structures in both cases of HEC (Fig. 1f and h) and HES (Fig. 1g). The results strongly support that the interparticle force in the presence of biobased polymer is the driving factor in the formation of network and dispersed structures with HEC and HES, respectively. Simulation confirmed that the strong attraction amongst silica nanoparticles in HEC solution may lead to diffusion limited aggregation (loose fractal structures), while the weak interactions among silica nanoparticles in HES solution result in reaction limited aggregation (close packed clusters). The qualitative differences observed in the simulated HEC and HES systems were complimented with a quantitative measure of cluster size at the 24 hour time point. The radius of gyration of individual

clusters was calculated in the 3D simulations. The results show the average radii of gyration to be 23 μm in HEC and 0.7 μm in HES, which in general agrees with experimental measurement of average cluster radii: 32 μm in HEC and 1.5 μm in HES. Due to limitations in image resolution, the precise measurement of radii is expected to be very challenging. The significant variation in cluster size amongst HEC and HES matrices highlights key differences in assembly, emphasizing qualitative similarity to the simulation result.

The drastic difference between the nanoparticle assembly structures inside HEC and HES suspensions, together with AFM and simulation results, suggest that the molecular architecture of the polymer backbone has profound effects upon the particle interactions and self-assembly. As discussed earlier, the morphology of HEC and HES in aqueous suspension can be drastically different, due to the conformational difference in how repeating units are connected. The extended conformation
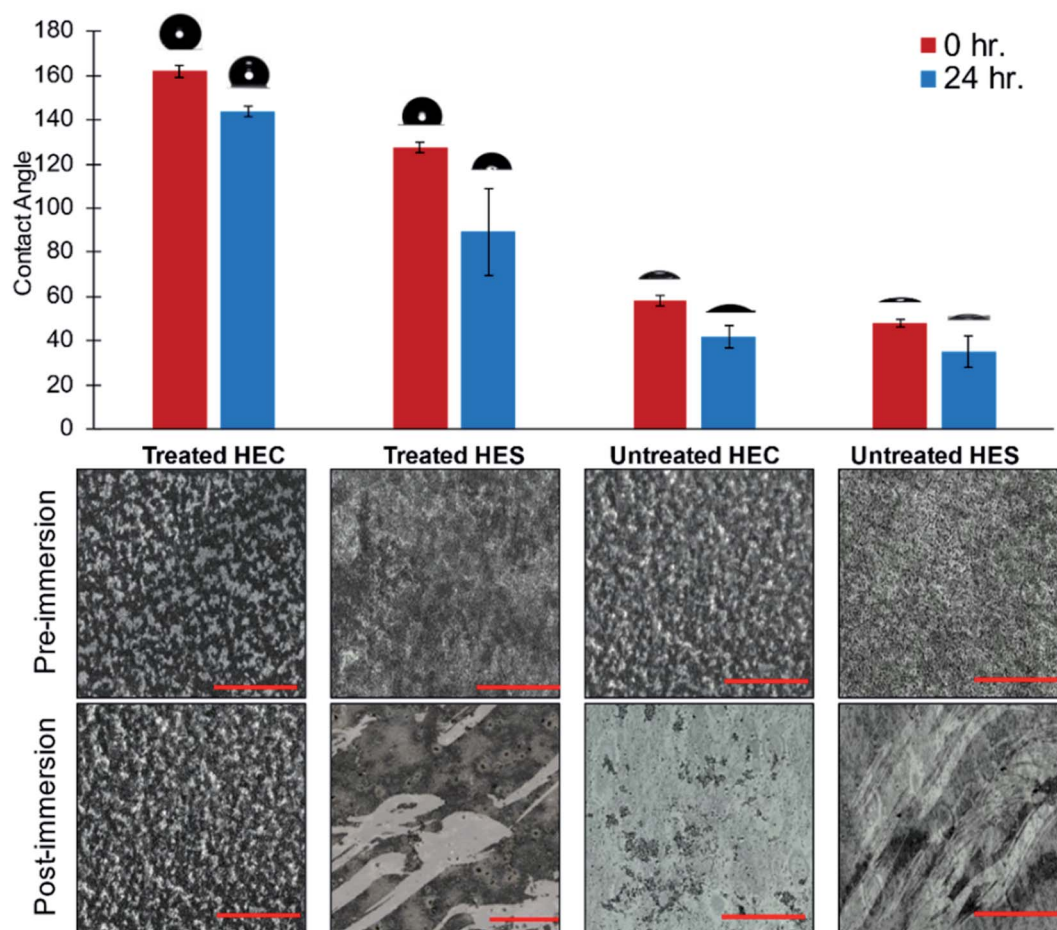
Fig. 3 Contact angle measurements and corresponding confocal optical images: fluorinated silane treated and untreated samples with 3% 100 nm silica pre and post immersion in water for 24 hours. Scale bar is 200 μm.

of HEC may induce stronger and longer-range attractions among silica surfaces than HES through hydrogen bonding and bridging effects. Another possible mechanism for attraction is the depletion force, which depends on many different factors including the polymer dimension and nanoparticle size.[39] It is known that larger polymer dimensions may induce stronger and longer-range depletion attractions amongst nanoparticles.[40] However, it is not entirely clear how polymer morphology would impact the depletion attractions. At this stage, the detailed mechanism is not yet clear how differences at the molecular level for HEC and HES lead to differences in the interactions medicated by these polymers, which warrants further studies in the future.

The unique structures formed by nanoparticles within HEC were utilized to create superhydrophobic surfaces. When nanoparticle loading is increased from 0.16 to 3 wt% in the formulation and a vaporized fluorinated silane treatment is applied after coating film is dried, a contact angle of 160° is observed (Fig. 2a). Silane treated HEC becomes hydrophobic due to surface bound water, which allows for silane to polymerize prior to its attachment to the coating surface. The observed clusters form due to a mismatch in energy between the polymer and unreacted water particles. The silane deposits in clusters to reduce the surface tension consideration.[60] Water repellency of formulation with HES under the same treatment condition is greatly reduced in comparison to HEC, with an angle of 127°. Without nanoparticles, the contact angle is reduced by 45° and 60° in HEC and HES, respectively. This suggests that nanoparticle assembly structures are essential in providing superhydrophobicity to the coatings.

Table 1 Crosshatch adhesion test performance metrics

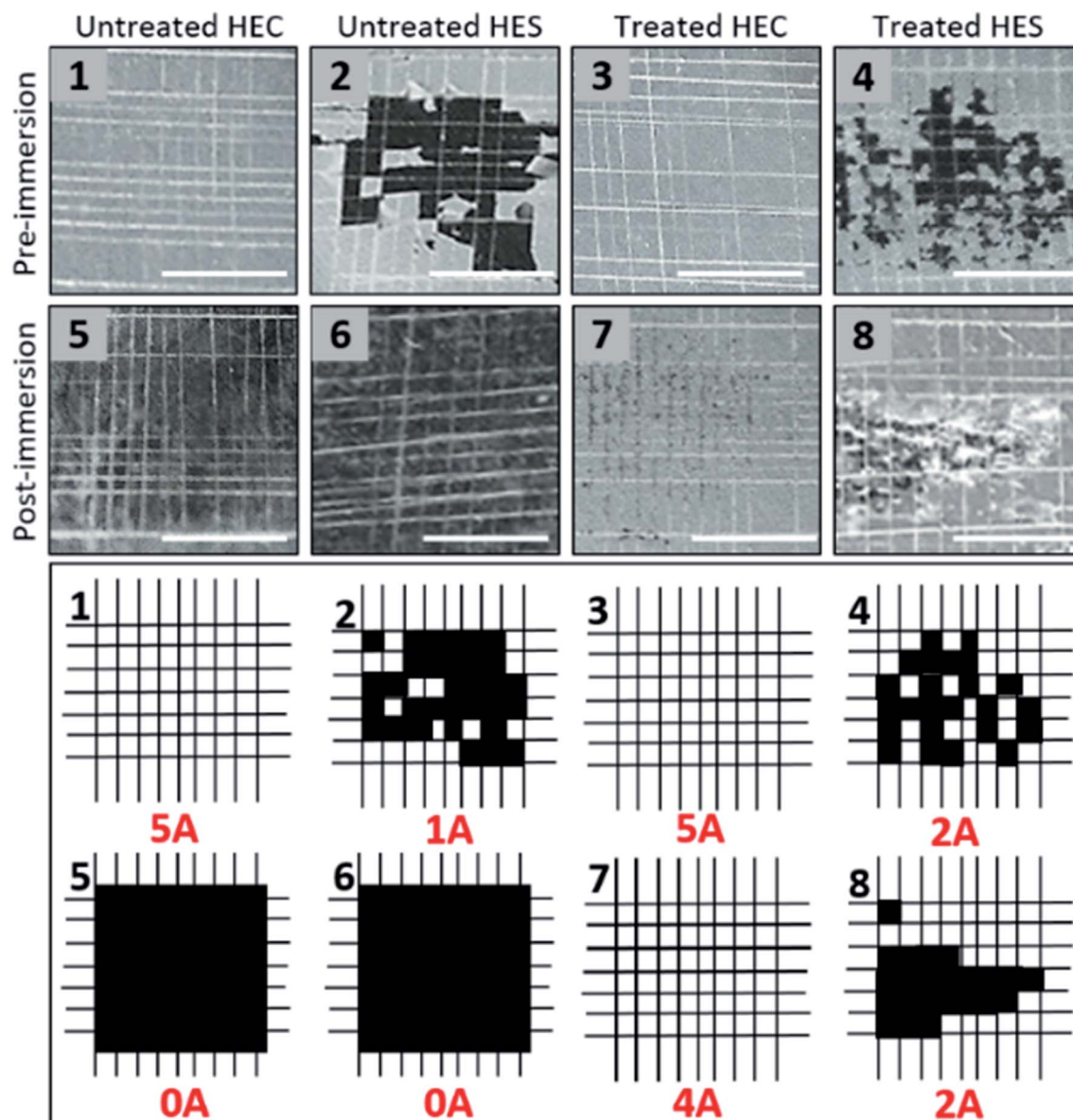| ASTM rating	Surface identifiers
5A	No peeling or removal
4A	Trace peeling or removal along incisions or at their intersection
3A	Jagged removal along incisions up to 1.6 mm (1/16 in.) on either side
2A	Jagged removal along most of incisions up to 3.2 mm (1/8 in.) on either side
1A	Removal from most of the area of the X under the tape
0A	Removal beyond the area of the X

Fig. 4 Adhesive crosshatch test and corresponding optical images of fluorinated silane treated samples with 3% 100 nm silica pre and post immersion in water for 24 hours. Ratings are assigned according to ASTM 3359. Scale bar is 10 mm.

Further characterization of the treated surface *via* SEM revealed that the silane vapor deposits as small clusters on the polymer coatings, in absence of nanoparticles. AFM topography measurements of the same surfaces reveal drastically different roughness profiles amongst HEC and HES treated coating surfaces (Fig. 2b). The HEC coatings presents much larger silane clusters than HES, likely contributing to its enhanced water repellency capability. With the introduction of the silica nanoparticles, SEM reveals multiscale roughness with fractal features in HEC. In HES, the nanoparticles are relatively dispersed, as they were in the dilute case. By contrast, in HEC the nanoparticles form heterogeneous assembly structures. The surface treated nanocomposites were then characterized using confocal microscopy as the surfaces are too rough for a successful AFM measurement. Confocal measurements corroborate the SEM data, exhibiting more than a three-fold enhancement in surface roughness with HEC compared to HES (Fig. 2c). The results are consistent with prior observations that surface roughness will enhance the hydrophobicity.[63–66] Further experiments demonstrate the importance of particle size, loading, and silane treatment. The results of these studies reveal that high loading of small particles promotes the best water repellency (Fig. S4†). Silica particle size does not drastically affect the contact angle, since surface roughness is mainly induced by particle assemblies, not individual particles. Non-fluorinated silane treatment, trichloro(octyl)silane, was also assessed in scope of this study (Fig. S5†). It was found that though this treatment can provide hydrophobicity, the fluorinated derivative is more effective. In all of the aforementioned cases, untreated samples showed poor water repellency, with and without nanoparticle filler.

The enhanced water repellency exhibited in the treated nanocomposites prompted studies of their robustness under extended wet conditions. In this batch of experiment, the coatings were applied to a flexible PET substrate. To test the water repellency, treated and untreated samples of HEC and HES with silica nanofiller were immersed in deionized water for 24 hours. The contact angle was measured post-immersion to reevaluate the coating performance. Obviously, the silane treatment was essential in providing heightened hydrophobicity to HEC and HES, but only HEC demonstrated comparable performance post-immersion. The contact angle of HES is diminished by 40° after immersion, whereas HEC only loses 15° (Fig. 3). With the trichloro(octyl)silane treatment, similar results are obtained pre- and post-immersion, with HEC contact angle reduced by 12°, and HES by 30° (Fig. S6†).

Confocal characterization of the surface reveals that adhesion is poor when the HEC and HES coatings are not treated with silane vapor, and the coating is washed away upon immersion. Interestingly, a similar phenomenon occurs even in treated HES, providing some explanation for its reduced contact angle post-immersion. HEC treated with fluorinated silane, on the other hand, retains its adhesion to the substrate after immersion for 24 hours (Fig. 3). Treatment with trichloro(octyl) silane shows the same trend, with only treated HEC maintaining adhesion post-immersion (Fig. S6†). Therefore, the fractal network structures assembled by silica nanoparticle in HEC not only provide the roughness required for superhydrophobic properties, but also offer the enhancement in adhesion. The structures are essential in retaining the adhesion performance even after extended immersion in water. This is not possible in the HES system, demonstrating the superior performance of HEC–silica coatings for water repellency applications.

An adhesive crosshatch test was further administered to further compare the adhesion performance of nanocomposite coatings. In order to carry out the test, the PET substrate was replaced with aluminum Q-panels. The crosshatch test is conducted by applying a crosshatch knife at a 90° angle. Subsequently, a piece of tape is quickly applied and removed from the crosshatched area. According to ASTM 3359, the performance of the coatings are assigned to one of the following rating based on their adhesion (Table 1):[67]

Without silane treatment (pre-immersion), HEC samples exhibit strong adhesion, with no removal of the coating from the substrate. Post-immersion, the coating was washed away. Interestingly, significant coating removal is observed in HES even prior to water immersion. Like HEC, post-immersion the coating is washed away, leaving no surface to be removed with the adhesion crosshatch method. After silane treatment, adhesion performance of both HEC and HES samples were improved. The HEC coating film demonstrates no coating removal prior to immersion, and very little afterwards. HES, on the other hand, exhibits jagged removal along the crosshatch before and after immersion, though generally the adhesion is improved compared to the untreated HES sample (Fig. 4). Again, the results of the adhesion test (along with contact angle and immersion) highlight the importance of nanoparticle assembly structures and polymer–nanoparticle interactions in determining macroscopic level material properties. The network structure formed with HEC polymers, and the roughness that is induced at high particle loading, have created a strongly adhered coating with superhydrophobic properties. The waterborne HEC coating demonstrates robustness to mechanical damage even under extended water immersion. The chemically identical HES polymer, was not capable of providing adhesion or superhydrophobic properties to the coating film. These results highlight the critical role of molecular conformation in determining the performance of products derived from biobased polymers.

Conclusion

In this study we present a waterborne biobased nanocomposite coating system composed of HEC and silica nanoparticles. It was demonstrated that the polymer morphology has a dramatic effect on the assembly of nanoparticles within the polymer matrix. Silica nanoparticles form small closed packed clusters dispersed uniformly in HES. By contrast, silica nanoparticles in HEC form fractal structures with long range connectivity. Liquid phase AFM revealed that assembly in HEC is driven by a large attraction force at a longer onset distance. Using AFM derived parameters for interparticle potential, computational simulations replicated the experimentally observed structures in HEC and HES systems. Furthermore, the assembled structures demonstrated great influence over the resulting water repellency and robustness of the coating. Upon silanization of the dried coating film, the HEC coating demonstrated superhydrophobicity (160° contact angle), with comparable performance post immersion in water for 24 hours. The observation is due to a multiscale roughness, in combination of the fractal nanoparticle assembly structures. Crosshatch testing further confirmed the robust adhesion performance of HEC nanocomposite coating. On the contrary, HES coatings performed poorly in adhesion, water repellency, and immersion robustness tests. Through this study we demonstrate that biobased polymer morphology can be used to influence nanoparticle assembly structures. High performing superhydrophobic coatings can be fabricated with water dispersible biobased polymers.

Author contributions

SJ designed and oversaw the project. EO designed and formulated the coating and performed all imaging and analysis with assistance from Y. Li. XY and JB designed and performed the simulation. CD and MT designed and performed silane treatment. GC and HT designed and performed contact angle measurement. RJ and Y. Liu designed and performed AFM measurement. All authors contributed to discussion and revision of the manuscript.

Conflicts of interest

There are no conflicts to declare.

Acknowledgements

References

1 C. L. Reichert, E. Bugnicourt, M.-B. Coltelli, P. Cinelli, A. Lazzeri, I. Canesi, F. Braca, B. M. Martinez, R. Alonso, L. Agostinis, S. Verstichel, L. Six, S. D. Mets, E. C. Gomez, C. Ißbrücker, R. Geerinck, D. F. Nettleton, I. Campos, E. Sauter, P. Pieczyk and M. Schmid, Bio-Based Packaging: Materials, Modifications, Industrial Applications and Sustainability, *Polymers*, 2020, **12**, 1558.

2 L. A. Heinrich, Future opportunities for bio-based adhesives – advantages beyond renewability, *Green Chem.*, 2019, **21**, 1866–1888.

3 E. Olson, F. Liu, T. Bahns, S. Jiang, K. Vorst and G. Curtzwiler, Post-consumer polymers (PCR) for color retention of delicatessen meats and elucidation of the light blocking mechanism, *Sustainable Mater. Technol.*, 2020, **25**, e00193.

4 G. Curtzwiler, E. Williams, A. Maples, N. Davis, T. Bahns, J. E. D. Leon and K. Vorst, Ultraviolet protection of recycled polyethylene terephthalate, *J. Appl. Polym. Sci.*, 2017, **134**, 45181–45188.

5 H. Lee, J. M. Koo, D. Sohn, I.-S. Kim and S. S. Im, High thermal stability and high tensile strength terpolyester nanofibers containing biobased monomer: fabrication and characterization, *RSC Adv.*, 2016, **6**, 40383–40388.

6 Z. Li, M. Rabnawaz and B. Khan, Response Surface Methodology Design for Biobased and Sustainable Coatings for Water- and Oil-Resistant Paper, *ACS Appl. Polym. Mater.*, 2020, **2**, 1378–1387.

7 D. A. Bellido-Aguilar, S. Zheng, Y. Huang, X. Zeng, Q. Zhang and Z. Chen, Solvent-Free Synthesis and Hydrophobization of Biobased Epoxy Coatings for Anti-Icing and Anticorrosion Applications, *ACS Sustainable Chem. Eng.*, 2019, **7**, 19131–19141.

8 G. Fredi, A. Dorigato, M. Bortolotti, A. Pegoretti and N. Bikiaris, Mechanical and Functional Properties of Novel Biobased Poly(decylene-2,5-furanoate)/Carbon Nanotubes Nanocomposite Films, *Polymers*, 2020, **12**, 2459.

9 P. Cataldi, P. Steiner, T. Raine, K. Lin, C. Kocabas, R. J. Young, M. Bissett, I. A. Kinloch and D. G. Papgeorgiou, Multifunctional Biocomposites Based on Polyhydroxyalkanoate and Graphene/Carbon Nanofiber Hybrids for Electrical and Thermal Applications, *ACS Appl. Polym. Mater.*, 2020, **2**, 3525–3534.

10 Z. Wang, P. Gnanasekar, S. S. Nair, R. Farnood, S. Yi and N. Yan, Biobased Epoxy Synthesized from a Vanillin Derivative and Its Reinforcement Using Lignin-Containing Cellulose Nanofibrils, *ACS Sustainable Chem. Eng.*, 2020, **8**, 11215–11223.

11 T. Xiang, S. Zheng, M. Zhang, H. R. Sadig and C. Li, Bioinspired Slippery Zinc Phosphate Coating for Sustainable Corrosion Protection, *ACS Sustainable Chem. Eng.*, 2018, **6**, 10960–10968.

12 F. A. G. S. Silva, F. Dourado, M. Gama and F. Poças, Nanocellulose Bio-Based Composites for Food Packaging, *Nanomaterials*, 2020, **10**, 2041.

13 M. Tian, X. Zhen, Z. Wang, H. Zou, L. Zhang and N. Ning, Bioderived Rubber–Cellulose Nanocrystal Composites with Tunable Water-Responsive Adaptive Mechanical Behavior, *ACS Appl. Mater. Interfaces*, 2017, **9**, 6482–6487.

14 T. Shen, P. Langan, A. D. French, G. P. Johnson and S. Gnanakaran, Conformational Flexibility of Soluble Cellulose Oligomers: Chain Length and Temperature Dependence, *J. Am. Chem. Soc.*, 2009, **2009**, 14786–14794.

15 I. K. Park, H. Sun, S. H. Kim, Y. Kim, G. E. Kim, Y. Lee, H. R. Choi, J. Suhr and J. D. Nam, Solvent-free bulk polymerization of lignin-polycaprolactone (PCL) copolymer and its thermoplastic characteristics, *Sci. Rep.*, 2019, **9**, 1–11.

16 S. Skovstrup, S. G. Hansen, T. Skrydstrup and B. Schiøtt, Conformational Flexibility of Chitosan: A Molecular Modeling Study, *Biomacromolecules*, 2010, **11**, 3196–3207.

17 A. C. O'Sullivan, Cellulose: the structure slowly unravels, *Cellulose*, 1996, **4**, 173–207.

18 S. Kobayashi, S. J. Schwartz and D. R. Lineback, Comparison of the structure of amylopectins from different wheat varieties, *Cereal Chem.*, 1986, **68**, 71–74.

19 E. Olson, Y. Li, F. Y. Lin, A. Miller, F. Liu, A. Tsyrenova, D. Palm, G. Curtzwiler, K. Vorst, E. Cochran and S. Jiang, Thin Biobased Transparent UV-Blocking Coating Enabled by Nanoparticle Self-Assembly, *ACS Appl. Mater. Interfaces*, 2019, **11**, 24552–24559.

20 M. D. Garrison and B. G. Harvey, Bio-based hydrophobic epoxy-amine networks derived from renewable terpenoids, *Appl. Polym. Sci.*, 2016, **133**, 43621–43633.

21 S. Jiang, A. V. Dyk, A. Maurice, J. Bohling, D. Fasano and S. Brownell, Design colloidal particle morphology and self-assembly for coating applications, *Chem. Soc. Rev.*, 2017, **46**, 3792–3807.

22 Y. Li, F. Liu, S. Chen, A. Tsyrenova, K. Miller, E. Olson, R. Mort, D. Palm, C. Xiang, X. Yong and S. Jiang, Self-Stratification of Amphiphilic Janus Particles at Coating Surfaces, *Mater. Horiz.*, 2020, **7**, 2047.

23 A. Tsyrenovaa, K. Miller, J. Yan, E. Olson and S. Jiang, Surfactant Mediated Assembly of Amphiphilic Janus Spheres, *Langmuir*, 2019, **35**, 6106.

24 J. Isrealachvili, *Intermolecular and Surface Forces*, Academic Press, Cambridge, MA, 3rd edn, 2015, p. 1084.

25 F. Liu, Y. Li, Y. Huang, A. Tsyrenova, K. Miller, L. Zhou, H. Qin and S. Jiang, Activation and Assembly of Plasmonic-Magnetic Nanosurfactants for Encapsulation and Triggered Release, *Nano Lett.*, 2020, **20**(12), 8773–8780.

26 F. Liu, S. Goyal, M. Forrester, T. Ma, K. Miller, Y. Mansoorieh, J. Henjum, L. Zhou, E. Cochran and S. Jiang, Self-assembly of Janus Dumbbell Nanocrystals and Their Enhanced Surface Plasmon Resonance, *Nano Lett.*, 2019, **19**(3), 1587–1594.

27 H. Lekkerkerker and R. Tuinier, *Colloids and the Depletion Interaction*, Springer Netherlands, Hiedelberg, Germany, 2011, p. 234.

28 J. Walz and A. Sharma, Effect of Long Range Interactions on the Depletion Force between Colloidal Particles, *J. Colloid Interface Sci.*, 1994, **168**, 485–496.

29 D. Ray, V. K. Aswal and J. Kohlbrecher, Micelle-induced depletion interaction and resultant structure in charged colloidal nanoparticle system, *J. Appl. Phys.*, 2015, **117**(16), 164310.

30 V. Tohver, J. E. Smay, A. Braem, P. V. Braun and J. A. Lewis, Nanoparticle halos: a new colloid stabilization mechanism, *PNAS*, 2001, **98**, 8950–8954.

31 S. Chen, E. Olson, S. Jiang and X. Yong, Nanoparticle assembly modulated by polymer chain conformation in composite materials, *Nanoscale*, 2020, **12**, 14560–14572.

32 Y. Li, S. Chen, S. Demirci, S. Qin, Z. Xu, E. Olson, F. Liu, D. Palm, X. Yong and S. Jiang, Morphology evolution of Janus dumbbell nanoparticles in seeded emulsion polymerization, *J. Colloid Interface Sci.*, 2019, **543**, 34–42.

33 M. Keyvan, Y. Liu, S. Bi, Y. Wang, J. Ren and M. Lu, Nonlinear cellular mechanical behavior adaptation to substrate mechanics identified by atomic force microscope, *Int. J. Mol. Sci.*, 2018, **19**, 3461.

34 C. Zhu, A. Soldatov and A. P. Mathew, Advanced microscopy and spectroscopy reveal the adsorption and clustering of Cu(II) onto TEMPO-oxidized cellulose nanofibers, *Nanoscale*, 2017, **9**, 7419–7428.

35 А. Петрус-Вилхелмус-Франсискус-Арис , К. М. ЛУСВАРДИ and Т. Т. НГУЙЕН , Hydroxyethyl cellulose substituted in mass, derivatives thereof, preparation method thereof and application, RU2007134407/05A, 2011.

36 S. Zheng, D. A. Bellido-Aguilar, X. Wu, X. Zhan, Y. Huang, X. Zeng, Q. Zhang and Z. Chen, Durable Waterborne Hydrophobic Bio-Epoxy Coating with Improved Anti-Icing and Self-Cleaning Performance, *ACS Sustainable Chem. Eng.*, 2018, **7**, 641–649.

37 J. O. F. West, G. W. Critchlow, D. R. Lake and R. Banks, Development of a superhydrophobic polyurethane-based coating from a two-step plasma-fluoroalkyl silane treatment, *Int. J. Adhes. Adhes.*, 2016, **68**, 195–204.

38 G. Saini, K. Sautter, F. E. Hild, J. Pauley and M. R. Linford, Two-silane chemical vapor deposition treatment of polymer (nylon) and oxide surfaces that yields hydrophobic (and superhydrophobic), abrasion-resistant thin films, *J. Vac. Sci. Technol.*, 2008, **26**, 1224.

39 M. A. Tshabalala, Wood surface modification by *in situ* sol–gel deposition of hybrid inorganic–organic thin films, in *Fifth International Woodcoatings Congress: Enhancing Service Life*, PRA Coatings Technology Centre, Prague, Czech Republic, 2006.

40 Y. Xie, C. A. S. Hill, Z. Xiao, H. Militz and C. Mai, Silane coupling agents used for natural fiber/polymer composites: a review, *Composites, Part A*, 2010, **41**, 806–819.

41 S. Oyola-Reynoso, Z. Wang, J. Chen, S. Çınar, B. Chang and M. Thuo, Revisiting the Challenges in Fabricating Uniform Coatings with Polyfunctional Molecules on High Surface Energy Materials, *Coatings*, 2015, **5**, 1002–1018.

42 P. Kothary, X. Dou, Y. Fang, Z. Gu, S.-Y. Leo and P. Jiang, Superhydrophobic hierarchical arrays fabricated by a scalable colloidal lithography approach, *J. Colloid Interface Sci.*, 2017, **487**, 484–492.

43 I. Y. Moon, B. H. Kim, H. W. Lee, Y.-S. Oh, J. H. Kim and S.-H. Kang, Superhydrophobic Polymer Surface with Hierarchical Patterns Fabricated in Hot Imprinting Process, *Int. J. Precis. Eng. Manuf.*, 2020, **7**, 493–503.

44 Y. Lee, S. H. Park, K. B. Kim and J. K. Lee, Fabrication of Hierarchical Structures on a Polymer Surface to Mimic Natural Superhydrophobic Surfaces, *Adv. Mater.*, 2007, **19**, 2330–2335.

45 E. Huovinen, J. Hirvi, M. Suvanto and T. A. Pakkanen, Micro–Micro Hierarchy Replacing Micro–Nano Hierarchy: A Precisely Controlled Way to Produce Wear-Resistant Superhydrophobic Polymer Surfaces, *Langmuir*, 2012, **28**, 14747–14755.

46 S. Kim, H.-J. Hwang, H. Cho, D. Choi and W. Hwang, Repeatable replication method with liquid infiltration to fabricate robust, flexible, and transparent, anti-reflective superhydrophobic polymer films on a large scale, *Chem. Eng. J.*, 2018, **350**, 225–232.

47 N. Okulova, P. Johansen, L. Christensen and R. Taboryski, Effect of Structure Hierarchy for Superhydrophobic Polymer Surfaces Studied by Droplet Evaporation, *Nanomaterials*, 2018, **8**, 831.

48 K. Maghsoudi, E. Vazirinasab, G. Momen and R. Jafari, Advances in the Fabrication of Superhydrophobic Polymeric Surfaces by Polymer Molding Processes, *Ind. Eng. Chem. Res.*, 2020, **59**, 9343–9363.

49 H. Yabu and M. Shimomura, Single-Step Fabrication of Transparent Superhydrophobic Porous Polymer Films, *Chem. Mater.*, 2005, **17**, 5231–5234.

50 L. Feng, S. Li, Y. Li, H. Li, L. Zhang, J. Zhai, Y. Song, B. Liu, L. Jiang and D. Zhu, Super-Hydrophobic Surfaces: From Natural to Artificial, *Adv. Mater.*, 2002, **14**, 1857–1860.

51 E. Bittoun and A. Marmur, The Role of Multiscale Roughness in the Lotus Effect: Is It Essential for Super-Hydrophobicity?, *Langmuir*, 2012, **28**, 13933–13942.

52 R. Zhu, M. Liu, Y. Hou, L. Zhang, M. Li, D. Wang, D. Wang and S. Fu, Biomimetic Fabrication of Janus Fabric with Asymmetric Wettability for Water Purification and Hydrophobic/Hydrophilic Patterned Surfaces for Fog Harvesting, *ACS Appl. Mater. Interfaces*, 2020, **12**, 50113–50125.

53 M. Toma, G. Loget and R. M. Corn, Flexible Teflon Nanocone Array Surfaces with Tunable Superhydrophobicity for Self-Cleaning and Aqueous Droplet Patterning, *ACS Appl. Mater. Interfaces*, 2014, **6**, 11110–11117.

54 A. Milionis, R. Ruffilli and I. S. Bayer, Superhydrophobic nanocomposites from biodegradable thermoplastic starch composites (Mater-Bi®), hydrophobic nano-silica and lycopodium spores, *RSC Adv.*, 2014, **4**, 34395–34404.

55 S. Zheng, D. A. Bellido-Aguilar, Y. Huang, X. Zeng, Q. Zhang and Z. Chen, Mechanically robust hydrophobic bio-based epoxy coatings for anti-corrosion application, *Surf. Coat. Technol.*, 2019, **363**, 43–50.

56 S. Ni, H. Zhang, P. M. Godwin, H. Dai and H. Xiao, ZnO nanoparticles enhanced hydrophobicity for starch film and paper, *Mater. Lett.*, 2018, **230**, 207–210.

57 M. P. Indumathi, K. S. Sarojini and G. R. Rajarajeswari, Antimicrobial and biodegradable chitosan/cellulose acetate phthalate/ZnO nano composite films with optimal oxygen permeability and hydrophobicity for extending the shelf life of black grape fruits, *Int. J. Biol. Macromol.*, 2019, **132**, 1112–1120.

58 B. Wang, J. Zhou, Z. Wang, S. Mu, R. Wu and Z. Wang, Cellulose nanocrystal/plant oil polymer composites with hydrophobicity, humidity-sensitivity, and high wet strength, *Carbohydr. Polym.*, 2020, **231**, 115739–115748.

59 H. M. Park, M. Misra, L. T. Drzal and A. K. Mohanty, "Green" Nanocomposites from Cellulose Acetate Bioplastic and Clay: Effect of Eco-Friendly Triethyl Citrate Plasticizer, *Biomacromolecules*, 2004, **5**, 2281–2288.

60 S. Oyola-Reynoso, I. D. Tevis, J. Chen, B. S. Chang, S. Cinar, J.-F. Bloch and M. Thuo, Recruiting Physi-sorbed Water in Surface Polymerization for Bio-Inspired Materials of Tunable Hydrophobicity, *J. Mater. Chem. A*, 2016, **4**, 14729–14738.

61 W. Banks, C. T. Greenwood, D. J. Hourston and A. R. Procter, Amylose in aqueous solution—a viscometric study, *Polymer*, 1971, **12**(7), 452–466.

62 W. Brown, D. Henley and J. Öhman, Studies on cellulose derivatives. Part II. The influence of solvent and temperature on the configuration and hydrodynamic behaviour of hydroxyethyl cellulose in dilute solution, *Die Makromolekulare Chemie*, 1963, **64**(1), 49–67.

63 N.-X. Zhu, Z.-W. Wei, C.-X. Chen, D. Wang, C.-C. Cao, Q.-F. Qiu, J.-J. Jiang, H.-P. Wang and C.-Y. Su, Self-Generation of Surface Roughness by Low-Surface-Energy Alkyl Chains for Highly Stable Superhydrophobic/Superoleophilic MOFs with Multiple Functionalities, *Angew. Chem., Int. Ed.*, 2019, **58**, 17033–17040.

64 J. Peng, X. Zhao, W. Wang and X. Gong, Durable Self-Cleaning Surfaces with Superhydrophobic and Highly Oleophobic Properties, *Langmuir*, 2019, **35**, 8404–8412.

65 A. Baidya, S. Kumar, D. Robin, H. A. Ras and T. Pradeep, Fabrication of a Waterborne Durable Superhydrophobic Material Functioning in Air and under Oil, *Adv. Mater. Interfaces*, 2018, **5**, 1701523.

66 Y. Li, F. Liu, S. Chen, A. Tsyrenova, K. Miller, E. Olson, R. Mort, D. Palm, C. Xiang, X. Yong and S. Jiang, Self-stratification of amphiphilic Janus particles at coating surfaces, *Mater. Horiz.*, 2020, **7**(8), 2047–2055.

67 ASTM, *Standard Test Methods for Measuring Adhesion by Tape Test*, ASTM International, West Conshohocken, PA, 2014, vol. D3359–09, pp. 1–8.